Nanoscale Advances

ROYAL SOCIETY OF CHEMISTRY

PAPER

View Article Online
View Journal | View Issue

Cite this: *Nanoscale Adv.*, 2026, **8**, 1322

Demonstration of the photo-controllability of the bistable opsin OPN5 using upconversion nanoparticles with multiple emission peaks upon near-infrared photoexcitation

Fukue Kotegawa,[a] Mari Takahashi,[a] Koichi Higashimine,[b] Yuichi Hiratsuka,[a] Kazuaki Matsumura,[a] Daisuke Kojima[c] and Shinya Maenosono*[a]

Received 1st December 2025
Accepted 8th January 2026

DOI: 10.1039/d5na01109d

rsc.li/nanoscale-advances

Upconversion nanoparticles (UCNPs) have emerged as promising tools for deep tissue optogenetics because they can convert near-infrared (NIR) light, which has high biopermeability, into ultraviolet (UV) or visible light. In optogenetics, microbially derived photoreceptor proteins such as channelrhodopsin (ChR) have been widely used. G protein-coupled receptor (GPCR)-type opsins have signal amplification capabilities and are emerging as promising candidates for high-sensitivity optogenetic tools. Since many GPCR-type opsins are so-called "bistable opsins" that can be switched between active and inactive states using light, it is not obvious whether multi-wavelength light from UCNPs can control bistable opsins. In this study, we constructed HEK293T cells expressing OPN5, a type of bistable opsin, and bound $NaYF_4$:Yb,Tm@$NaLuF_4$ core–shell UCNPs onto the cells. It was then demonstrated that light emitted from UCNPs upon NIR irradiation can control OPN5 even when the wavelengths that activate and deactivate OPN5 are simultaneously emitted.

Introduction

Over the past two decades, optogenetics has developed significantly, particularly in the field of neuroscience, and is now one of the main techniques used in life science research. Channelrhodopsins (ChRs) are light-gated ion channel proteins derived from *Chlamydomonas reinhardtii*, and optogenetics began in 2005 when Boyden *et al.* succeeded in controlling action potentials in ChR-expressing neurons using blue light irradiation.[1] Since then, various photoreceptor proteins have been discovered and microbially derived photoreceptor proteins (type 1 opsins) such as ChR2 (ref. 2–4) and halorhodopsin[5,6] have been widely used as the main tools in optogenetics. In microbial ChRs, the chromophore retinal is photo-isomerized from all-*trans* retinal to 13-*cis* retinal by light absorption, which then triggers a series of reaction steps that open the channel. After a short time (within tens of seconds), the channel spontaneously closes to return to the original dark state.[7,8] Since it is possible to induce rapid changes in electrical potential through optical stimulation, it is useful for controlling the on/off of neural activity.

On the other hand, in animals, there are many opsins (type 2 opsins) that are responsible for non-visual physiological responses. Many of these are G-protein coupled receptor (GPCR)-type, which are known to induce intracellular signaling cascades in response to light stimulation, and be involved in the regulation of a diverse array of physiological functions such as neural activity,[9] metabolism,[10] hormone secretion,[11] and circadian rhythms.[12] To date, thousands of opsins have been identified. Those which use 11-*cis* retinal as a chromophore and transmit information *via* G proteins are classified into at least six subfamilies, each of which activates a specific G protein subtype.[13,14] These GPCR-type opsins induce cellular responses by activating G proteins in response to light, which causes the isomerization of retinal from 11-*cis* to all-*trans*.[15,16] GPCR-type opsins have the potential to be used as tools for optogenetic control of various physiological responses. Furthermore, they are characterized by their ability to amplify signals. Thus, when used as optogenetic tools, they are expected to provide high sensitivity.

Some GPCR-type opsins (*e.g.* vertebrate visual opsins) are difficult to reuse because after activation by light stimulation the spontaneous detachment of the chromophore then renders them inactive.[13,17,18] However, many GPCR-type opsins can be induced to a stable active state by light stimulation, and then returned to an inactive state by irradiating them with light of a different wavelength.[13,19] Such opsins are called "bistable opsins" and, due to their reusability, have potential for

[a]*School of Materials Science, Japan Advanced Institute of Science and Technology, 1-1 Asahidai, Nomi, Ishikawa 923-1292, Japan. E-mail: shinya@jaist.ac.jp*
[b]*Center for Nano Materials and Technology, Japan Advanced Institute of Science and Technology, 1-1 Asahidai, Nomi, Ishikawa 923-1292, Japan*
[c]*Department of Biological Sciences, School of Science, The University of Tokyo, 7-3-1 Hongo, Bunkyo-ku, Tokyo 113-0033, Japan*

application as optogenetic tools.[20–22] For example, it has been reported that mouse and human melanopsins exhibit bistable-like characteristics, being activated by blue light (wavelength $\lambda \sim 470$ nm) and deactivated by yellow light ($\lambda \sim 560$ nm).[23,24] Parapinopsin, which is expressed in the pineal organ of fish, is a bistable opsin that is activated by UV light ($\lambda \sim 370$ nm) and deactivated by green light ($\lambda \sim 515$ nm).[25] Neuropsin (OPN5) in chickens, mice and humans is also a bistable opsin that is activated by UV light ($\lambda \sim 380$ nm) and deactivated by blue light ($\lambda \sim 470$ nm).[26,27] Surprisingly, it has been found to be expressed in the deep brain and internal organs,[27,28] and in addition to its visual functions, including its effect of suppressing myopia,[29] it has been reported to be involved in thermogenesis in brown adipose tissue[30] and melanin formation in the pituitary gland.[31] Recently, Wietek *et al.* reported that the ciliary opsin of *Platynereis dumerilii* (*Pd*CO) is a bistable opsin that is activated by UV/blue light ($\lambda \sim 360$–405 nm) and deactivated by green light ($\lambda \sim 525$ nm), and has the potential to inhibit synaptic transmission with high temporal precision.[22]

There are still many unknowns about the physiological role and signaling mechanisms of bistable opsins. However, because conventional optogenetics involves directly irradiating the target area with the stimulus light, the short-wavelength light (UV or blue light) is strongly affected by light scattering and absorption within living tissue, thus there are problems with low biopermeability and high phototoxicity.[32–34] Therefore, in order to expand the applications of bistable opsins in optogenetics in the future, it will be important to develop non-invasive, spatially precise optical control technology.

Upconversion nanoparticles (UCNPs) are nanomaterials that can convert near-infrared (NIR) light, which has high biopermeability,[35] into shorter wavelengths such as UV/visible light. Therefore, after delivery and accumulation of UCNPs to the desired location within a living tissue, it is possible to generate UV/visible light locally and selectively by irradiating NIR light from outside the tissue, thus enabling non-invasive and spatially precise light control. NIR-to-UV/visible wavelength conversion using UCNPs inside biological tissue has been applied in various fields of life science, including optogenetics,[36–40] therapy,[41,42] bioimaging,[43,44] and biosensing.[45,46] Most previous optogenetic studies using UCNPs have used ChRs as tools,[36–40] and to the best of our knowledge, there have been no studies using GPCR-type bistable opsins.

However, when considering the idea of optically stimulating bistable opsins such as parapinopsin, OPN5 and *Pd*CO (which are activated by UV light) using the emission of UCNPs, a troublesome problem arises. Namely, UCNPs that can emit UV light upon NIR light excitation often have even stronger emission in the blue to green region at the same time.[47–54] Problematically, this by-product light is often the wavelength of light that deactivates bistable opsins. When using ChR as an optogenetic tool, even if the UCNPs have multiple emission wavelengths, there is no major problem as long as the ChR activation wavelength is included. However, it is not obvious whether it is actually possible to control bistable opsins using UCNPs with multi-wavelength emission. Since it is extremely difficult in principle to create UCNPs that emit monochromatic UV light, given the emission mechanism, this problem is unavoidable when trying to control bistable opsins using UCNPs.

In this study, we used OPN5, a bistable opsin, as a model and examined whether it is possible to control OPN5 with light emitted by UCNPs under NIR light irradiation, using OPN5-expressing HEK293T cells. The results demonstrated that when UCNPs were bound to the cell surface, they could activate OPN5 through the light emitted from the UCNPs. This result shows the feasibility of non-invasive, selective, and local optical control of bistable opsins using UCNPs.

Results and discussion

Structure and optical properties of UCNPs

In this study, we synthesised $NaYF_4$:Yb,Tm@$NaLuF_4$ core–shell UCNPs. Experimental details are in the SI. TEM images of as-synthesised $NaYF_4$:Yb,Tm core UCNPs (Fig. 1a) show that they are monodisperse hexagonal prisms with a mean size of 63.4 ± 2.1 nm. Fig. 1b shows a TEM image of as-synthesised $NaYF_4$:Yb,Tm@$NaLuF_4$ core–shell UCNPs. The mean size increased to 88.9 ± 4.0 nm, suggesting that a shell with a thickness of approximately 13 nm was formed. The HAADF-STEM image (Fig. 1c) and STEM-EDS elemental maps (Fig. 1d–j) of the core–shell UCNPs proved that the $NaLuF_4$ shell was formed uniformly. Shell formation reduces the effect of surface defect levels, dramatically improving the emission efficiency – since defect levels cause a loss of energy during transfer from the sensitizer (Yb^{3+}) to the activator (Tm^{3+}).[47] All UCNPs are hexagonal β-$NaYF_4$ phase, and there are no impurity phases or crystal phase transitions due to shell formation (Fig. 1k). Fig. 1l shows the emission spectra of core and core–shell UCNPs dispersed in hexane and photographs of the samples under NIR laser irradiation. For reference, the absorption spectra of inactive and active OPN5 are shown in Fig. S1 in the SI. The conversion efficiency of the core–shell UCNPs was improved about a hundredfold compared to the core UCNPs. As can be seen from the inset of Fig. 1l, the relative intensities of each emission peak did not change significantly, indicating no particular change in the wavelength conversion mechanism (Fig. 1m). In the following experiments, we used only core–shell UCNPs.

Encapsulation of UCNPs with phospholipids

Since as-synthesised UCNPs are hydrophobic, we encapsulated them using PEGylated phospholipids (DOPE-PEG350) and biotinylated phospholipids (Biotin-DOPE) (Fig. 2a) to impart water dispersibility and biocompatibility (Fig. 2b). Experimental details are in the SI. Encapsulated UCNPs are hereafter denoted as UCNP@Biotin. The hydrodynamic size distribution and zeta potential (ζ) of UCNP@Biotin in water (pH = 7) are shown in Fig. 2c and d, respectively. The average hydrodynamic size (D_H) was 117 nm, which is almost the same as the theoretical geometric size of the UCNPs (approx. 100 nm, considering the molecular lengths of oleic acid (2.2 nm) and phospholipids (≈3 nm)), suggesting that most UCNPs are individually encapsulated and have high dispersibility. The broad D_H distribution is

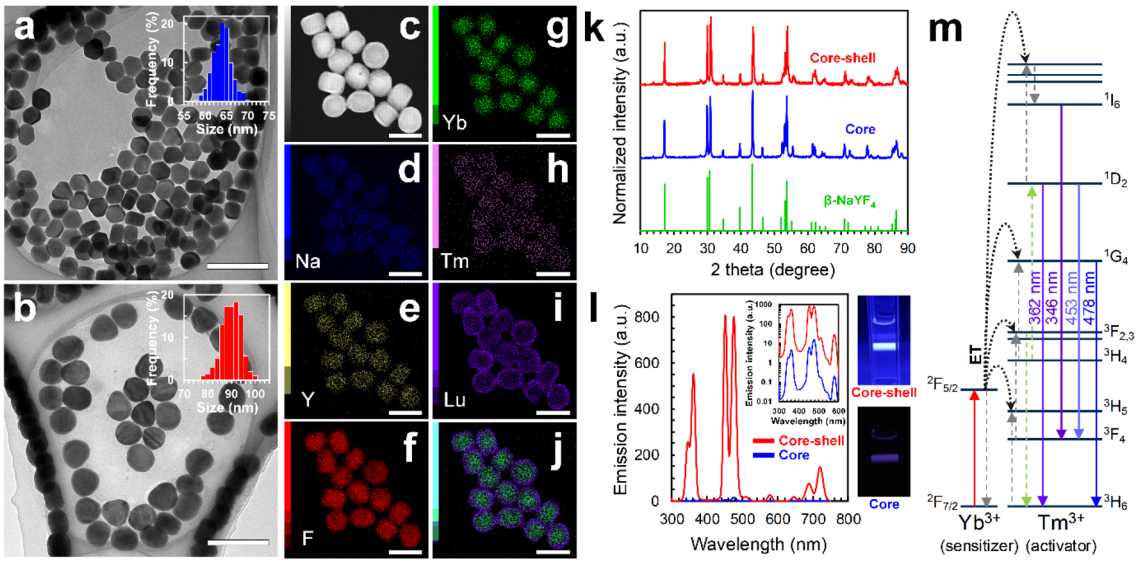

Fig. 1 TEM images of (a) as-synthesised core and (b) core–shell UCNPs. Scale bars are 200 nm. The insets inserted show particle size distribution histograms obtained from 300 randomly selected particles. (c) HAADF-STEM image and (d–j) EDS maps of core–shell UCNPs. (d) Na Kα line, (e) Y Kα line, (f) F Kα line, (g) Yb Lα line, (h) Tm Lα line, (i) Lu Lα line, and (j) overlay of Yb and Lu. Scale bars are 100 nm. (k) XRD patterns of core and core–shell UCNPs. The reference pattern is hexagonal β-$NaYF_4$ (ICDD PDF no. 00-016-0334). (l) Emission spectra and photographs of hexane dispersions of core (98 μg mL^{-1}) and core–shell UCNPs (300 μg mL^{-1}) when irradiated with NIR laser light (the number of UCNPs was adjusted to be equal). The inset is a semi-log plot of the main emission peak region. (m) Photophysical mechanism of wavelength conversion in the $NaYF_4$:Yb,Tm UCNP.

presumably due to result from the coexistence of phospholipid liposomes and UCNP–phospholipid hybrids. The value of ζ was −22.6 mV. Fig. 2e shows the emission spectrum of water-dispersed UCNP@Biotin under NIR laser irradiation. The relative intensities of each emission peak did not change, indicating no particular changes in the wavelength conversion mechanism, but the conversion efficiency was significantly lower than when dispersed in hexane (Fig. 1l). This is a well-known phenomenon, and the main causes are the promotion of non-radiative recombination, and absorption of NIR light by water molecules.[55]

Binding of UCNPs to cells

To create OPN5-expressing HEK293T cells (OPN5-HEK), we constructed an OPN5 plasmid with a FLAG tag on the outside of the cell using a snorkel structure (Fig. S2). Experimental details are in the SI. The idea being to bind UCNPs to the cell *via* the FLAG tag (Fig. S3). We transfected this OPN5 plasmid into HEK293T cells and created OPN5-HEK. To confirm that the OPN5-HEK were produced as designed, we confirmed that the FLAG tag was presented extracellularly by immunostaining without membrane permeabilization (Fig. S4a and b). On the other hand, when membrane permeabilization was performed, stronger signals were observed (Fig. S4c and d), suggesting that

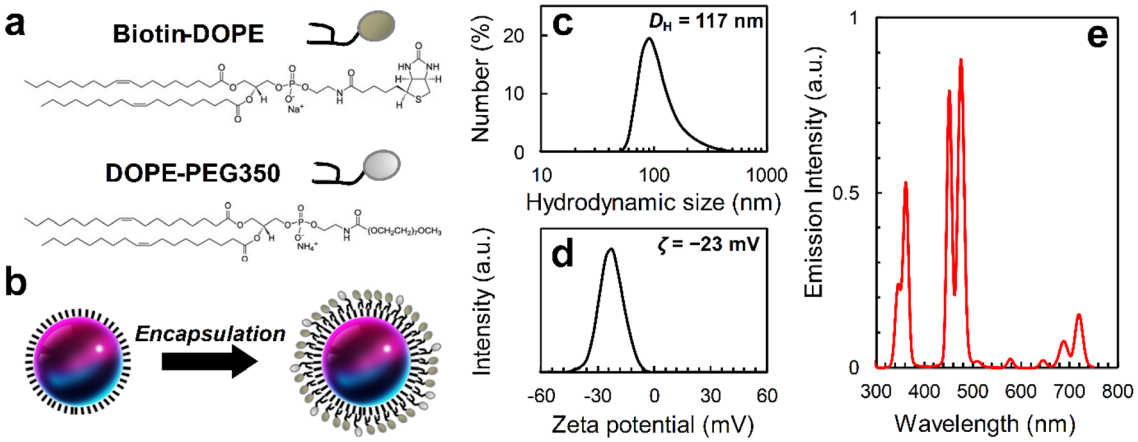

Fig. 2 (a) Molecular structure of Biotin-DOPE and DOPE-PEG350 and (b) schematic diagram of encapsulation. (c) Hydrodynamic size distribution, (d) zeta potential, and (e) emission spectrum of water-dispersed UCNP@Biotin.

some OPN5 did not undergo membrane transport and remained in the cytoplasm. This is quite possible for membrane proteins such as GPCRs.[56] The transfection efficiency was found to be approximately 9%, and the percentage of cells expressing FLAG extracellularly was approximately 5%. As shown in Fig. S3, a biotinylated anti-FLAG antibody and streptavidin were sequentially bound to FLAG, with the UCNP@Biotin finally bound to the streptavidin *via* the biotin–avidin interaction.

We tried to confirm whether UCNP@Biotin was actually binding to cells, but when we irradiated the cells with NIR laser and observed the UCNP emission through a DAPI filter, the light of the NIR laser's second-harmonic scattering hid the UCNP emission, making it indistinguishable. Therefore, when performing fluorescence microscopy observations under NIR laser light irradiation, it is necessary to be aware of the effects of NIR light and take the utmost care. Therefore, the binding of UCNP@Biotin to OPN5-HEK was confirmed by TEM observation of UCNP@Biotin-treated OPN5-HEK (Fig. S5). In the subsequent Ca^{2+} imaging experiments, fluorescence imaging was performed with the excitation light turned off. During the course of this experiment, although some cell proliferation was observed, no cell death nor any obvious cytotoxicity were observed. Furthermore, the MTT assay results also showed no significant cytotoxicity, as shown in Fig. S6.

Ca^{2+} imaging

Sugiyama *et al.* reported that OPN5 causes a transient increase in intracellular Ca^{2+} concentration (C_{Ca}) in response to UV light stimulation.[57] Therefore, we first irradiated OPN5-HEK with UV light ($\lambda = 365$ nm) (case 1) to confirm whether we could control OPN5 in the same way as in previous reports. Fig. 3a shows the difference image obtained by subtracting the pre-irradiation fluorescence image from the post-irradiation fluorescence image of Fluo-4 in OPN5-HEK after 8 s of UV irradiation. Experimental details are in the SI. An increase in C_{Ca} was observed in many cells. The average value of the fluorescence intensity for the 1 min before light stimulation was defined as F_0, and the cells that showed an increase in fluorescence intensity, $F(t)$, of $\geq 1.2F_0$ were defined as "responding cells". In the case of UV light irradiation, for example, the number of responding cells ($N_{responding}$) was 68 and the number of cells expressing FLAG extracellularly ($N_{available}$) was estimated to be about 120 (calculated from the percentage of cells expressing FLAG extracellularly), so the response ratio ($P_{res} = 100 \times N_{responding}/N_{available}$) was calculated to be 57%. Table 1 shows the mean P_{res} value and its 95% confidence interval obtained from three experiments conducted under identical conditions. The results of the other two replication experiments conducted under identical conditions are shown in Fig. S7 and S8. Typical difference images for cases 2 and 4 are also shown in Fig. S9. For case 3, difference images taken at 10 second intervals from 11 seconds to 51 seconds after the completion of NIR irradiation are shown in Fig. S10 for all three experiments. To accurately calculate P_{res}, we attempted several methods to determine $N_{responding}$ by fluorescently labelling OPN5 or FLAG tags. Unfortunately, none of these attempts were successful. Fig. 3b plots the average value of $F(t)/F_0$ for all responding cells ($\bar{F}$). The behavior of $F(t)/F_0$ in individual cells was similar to that shown in Fig. 3b, with little variation in the rate of increase or decay, except for the maximum value of $F(t)/F_0$. The Ca^{2+} response was similar to that reported by Sugiyama *et al.*,[57] with $F(t)/F_0$ reaching its maximum value immediately after UV irradiation and then returning to its original state over the next 20–30 s, confirming that OPN5 was functioning normally. Intermittent irradiation of OPN5-HEK with UV light (Fig. S11) over a period of 20 minutes demonstrated that the Ca^{2+} response was repeatable. Adding calcimycin immediately after the Ca^{2+} imaging experiment, we estimated the maximum Ca^{2+} response F_{max}, and found that $F_{max}/F_0 = 3.4$–6.0. Therefore, it is thought that UV light irradiation increased C_{Ca} to around 40–80% of the upper limit.

The Ca^{2+} response when NIR laser light was irradiated on OPN5-HEK in the absence of UCNP@Biotin (case 2) is shown in Fig. 3c ($P_{res} = 5.0 \pm 2.0\%$, see Table 1). Surprisingly, 5% of OPN5-HEK showed a Ca^{2+} response when exposed to NIR laser light. We will discuss the reason for this later. The behavior of $F(t)/F_0$ of individual cells was similar to that in Fig. 3c, except for the maximum value. Unlike case 1, $F(t)/F_0$ reached its maximum value 10 s after the NIR laser light was turned off, and then returned to its original state over the next 20–30 s.

Fig. 3d shows the Ca^{2+} response of OPN5-HEK with bound UCNP@Biotin under NIR laser light irradiation (case 3) ($P_{res} = 15.0 \pm 3.1\%$, see Table 1). Unlike both case 1 and case 2, $\bar{F}$ reached its maximum value 20 s after the NIR laser light was turned off, and then gradually returned to its original state over the next 30–60 s. Additionally, there was a lot of variation in the behaviour of $F(t)/F_0$ in individual cells, so the time courses of $F(t)/F_0$ for all responding cells is shown in Fig. S12. Note that although the same experiment was repeated three times, Fig. S12 shows the results from the first experiment in case 3 as an example. For comparison, Fig. 3e shows the Ca^{2+} response when 200 μg of UCNP@Biotin was simply added to the dish (case 4) (without the anti-FLAG antibody or streptavidin). In this case, the Ca^{2+} response was similar to that in case 2 (Fig. 3c). Fig. 3f is a graph that overlays Fig. 3c–e to facilitate comparison, focusing on the time period in which a Ca^{2+} response was observed. Note that in case 3, after adding 200 μg of UCNP@-Biotin, the dish was washed twice, but in case 4, no washing was performed, so the amount of UCNP@Biotin in the dish was overwhelmingly lower in the former, but the value of P_{res} was four times higher. The cause of the differences in the value of P_{res} for each case is explained briefly in the SI.

Fig. 3g and h show the results of control experiments in which OPN5-HEK was irradiated with NIR light in the absence of 11-*cis* retinal (11cR) (case 5) and untreated HEK293T (case 6), respectively. No Ca^{2+} response was observed in either case. From these results and the result of case 2 (Fig. 3c), the reasons for the observed Ca^{2+} response of OPN5-HEK to NIR light irradiation is probably due to the isomerization of 11cR caused by either a temperature increase or multiphoton absorption. Regarding the former, it has been reported that *Drosophila* rhodopsin has two roles: photoreception and thermoreception, suggesting a potential for response to a temperature increase

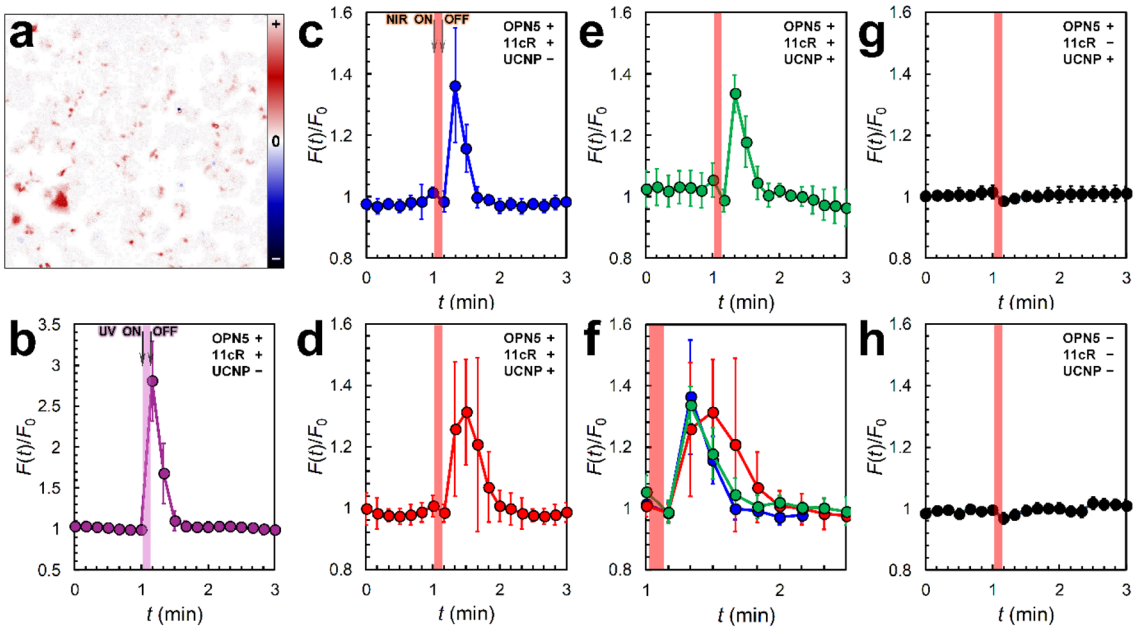

Fig. 3 Results of Ca^{2+} imaging. (a) Difference fluorescence images before and after UV irradiation of OPN5-HEK (after−before). Note that the post-irradiation fluorescence image refers to the fluorescence image captured 1 second after the completion of NIR light irradiation. The colour bar on the right has a centre of 0 (white), with colours above it representing positive differences and colours below it representing negative differences. (b) $\bar{F}$ when OPN5-HEK (−UCNP) was irradiated with UV light, (c) $\bar{F}$ when OPN5-HEK (−UCNP) was irradiated with NIR light, (d) $\bar{F}$ when OPN5-HEK (+UCNP (bound)) was irradiated with NIR light, and (e) $\bar{F}$ when OPN5-HEK (+UCNP (unbound)) was irradiated with NIR light. (f) Graph plotted by overlaying panels (c)–(e). (g) Average $F(t)/F_0$ for 100 randomly-selected cells in OPN5-HEK (+UCNP (bound), −11cR) when irradiated with NIR light ($N_{responding} = 0$), and (h) average $F(t)/F_0$ for 100 randomly-selected cells in HEK293T cells when irradiated with NIR light ($N_{responding} = 0$).

caused by the strong NIR light.[58] Regarding the latter, it has been reported that 11cR may be isomerized by the multiphoton absorption of NIR light.[59] Table 1 summarizes all experimental conditions and P_{res} values with 95% confidence intervals.

Kinetic analysis of Ca^{2+} response

In general, C_{Ca} is kept low, at around 100 nM, and this is achieved through a complex interaction of various mechanisms including: ion pumps; Na^+/Ca^{2+} exchanger; chelating proteins; and Ca^{2+} channels. In addition to these natural Ca^{2+} transport mechanisms, in the case of OPN5-HEK, the GPCR-type bistable opsin OPN5 has been exogenously added. The mechanism by which OPN5 increases C_{Ca} has not been fully elucidated, but it has been reported that UV light stimulation drives the signaling pathway of the G_q protein α subunit, causing an increase in C_{Ca}.[60] It is also known that inositol triphosphate (IP_3) produced by the effector (phospholipase C) of the G_q-coupled receptor binds to the IP_3 receptor in the smooth endoplasmic reticulum (SER), causing Ca^{2+} to be released from the SER and increasing the C_{Ca}.[61]

Let us consider the reasons for the different Ca^{2+} response behaviors observed in cases 1 to 4. To do this, we first fitted the increase and decay portions of $F(t)/F_0$ with a logistic function

Table 1 Experimental conditions and P_{res} values for each case[a]

Case	Excitation light	OPN5	11cR	UCNP	Antibody	Avidin	P_{res}	95% CI
1	UV	+	+	−	−	−	61.9%	55.4–68.5%
2	NIR	+	+	−	+	+	5.0%	3.0–7.0%
3	NIR	+	+	+	+	+	15.0%	11.9–18.1%
3′	NIR	+	+	+	+	+	10%	N/A
4	NIR	+	+	+	−	−	3.6%	1.7–5.5%
5	NIR	+	−	+	+	+	0.3%	0.0–0.7%
6	NIR	−	−	−	−	−	0.0%	0.0–0.0%

[a] UCNP, antibody and avidin denote UCNP@Biotin, anti-FLAG antibody and streptavidin, respectively. P_{res} value varies slightly each time. For cases other than case 3′, the P_{res} value is the average of three experiments conducted under identical conditions. The 95% CI refers to the 95% confidence interval for P_{res}. In another experiment corresponding to case 3 (case 3′), the cell seeding number was increased (2.8×10^5 cells per dish).

(eqn (1)) and an exponential decay function (eqn (2)), respectively.

$$\frac{F(t)}{F_0} = 1 + \frac{K}{1 + A\mathrm{e}^{-rt}} \quad (1)$$

$$\frac{F(t)}{F_0} = 1 + \alpha\mathrm{e}^{-\beta t} \quad (2)$$

where A and α are constants, K is the carrying capacity, r is the intrinsic rate of increase, β is the decay constant, and t is time. In the fitting, the values of K and A were all set to constants, and r, α, and β were used as the fitting parameters. As an example, the fitting results of $F(t)/F_0$ for all responding cells in case 3 are shown in Fig. S12. The values of r and β obtained by fitting the Ca^{2+} responses of all responding cells in cases 1 to 4 are summarized in the phase diagram in Fig. 4a. Experiments cases 1–4 were each performed three times under identical conditions. Fig. 4a plots all data obtained from the three repeated experiments, showing consistent results that confirm reproducibility (for details see Table S1). As can be seen from Fig. 4a, the values of r can be divided into three main groups. Case 1 showed the largest r (r_{high}). Half of the responding cells in case 3 showed the smallest r (r_{low}). The remaining half of the responding cells in case 3, as well as cases 2 and 4, showed an intermediate r (r_{mid}). Crucially, the responding cells exhibiting r_{low} were observed only in case 3; no responding cells with r_{low} were observed in any other case (see also Table S1). In addition, the ratio of the number of cells with r_{low} to the number with r_{mid} in case 3′ (another experiment corresponding to case 3) was almost the same as that in case 3, demonstrating high reproducibility (Fig. S13). There was a large variation in β, arising from the complexity of processes involved in returning to a steady C_{Ca}.

If C_{Ca} is returned to its original state by the various cell mechanisms mentioned previously, then we can assume that r is proportional to the number of activated OPN5. Considering all the factors involved in the activation and deactivation of OPN5 (Fig. 4b), the following reaction rate equation is obtained:

$$\frac{\mathrm{d}\phi_a}{\mathrm{d}t} = k_{UV}\phi_i + k_{NIR}\phi_i - k_{Blue}\phi_a - k_{Dark}\phi_a \quad (3)$$

where ϕ_a and ϕ_i denote the fractions of active and inactive OPN5 in a single cell, respectively ($\phi_a + \phi_i = 1$). k_{UV}, k_{NIR}, k_{Blue}, and k_{Dark} represent the rate constants for UV light activation, NIR light activation, blue light deactivation, and dark deactivation, respectively. From the experimental results, we can assume that $k_{NIR} \ll k_{UV}$. In addition, in the case of the bistable opsin OPN5, k_{Dark} is sufficiently small compared to the other rate constants, so we assumed that $k_{Dark} \approx 0$. Therefore, the rate equations for cases 1 to 3 are expressed as eqn (4)–(6), respectively.

$$\frac{\mathrm{d}\phi_a}{\mathrm{d}t} = k_{UV}\phi_i \quad (4)$$

$$\frac{\mathrm{d}\phi_a}{\mathrm{d}t} = k_{NIR}\phi_i \quad (5)$$

$$\frac{\mathrm{d}\phi_a}{\mathrm{d}t} = k_{UV}\phi_i + k_{NIR}\phi_i - k_{Blue}\phi_a \quad (6)$$

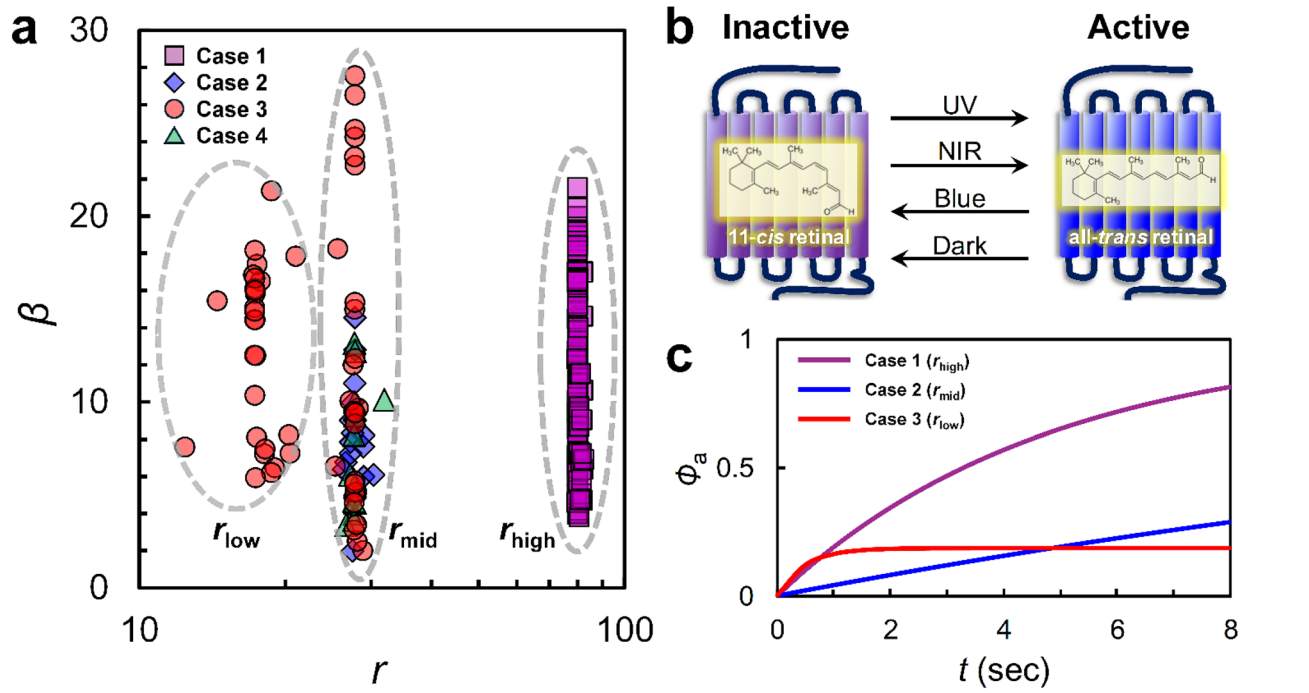

Fig. 4 Kinetic analysis results of Ca^{2+} imaging. (a) Phase diagram of r and β obtained by fitting the Ca^{2+} responses of all responding cells in cases 1 to 4. All data from three repeated experiments are plotted. For details, see Table S1. (b) Schematic diagram of activation and deactivation of bistable opsin OPN5. (c) Example of calculated time course of ϕ_a during 8 s of excitation light irradiation for cases 1 to 3 with the initial conditions $\phi_a(0) = 0$ and $\phi_i(0) = 1$.

Of course, k_{UV}, k_{NIR} and k_{Blue} are closely related to factors such as light intensity, absorbance and quantum yield. For the sake of simplicity, we will not mention the exact physical factors but instead treat them as comprehensive rate constants that include physical factors. Based on the assumption that $r \propto \phi_a$, it is thought that r is proportional to ϕ_a after 8 s of light irradiation. The average values of r_{high}, r_{mid}, and r_{low} are 80.9, 28.2, and 18.5, respectively. When each rate constant was fitted so that the ratio of ϕ_a after 8 s of irradiation would be 80.9 (case 1): 28.2 (case 2): 18.5 (case 3), the values of k_{UV}, k_{NIR} and k_{Blue} were determined to be 0.2, 0.042, and 1.05, respectively (note that these values are not unique). Using these rate constants, the time variation of ϕ_a during excitation light irradiation was calculated for cases 1 to 3, and the results are shown in Fig. 4c. In case 3, since UCNPs emit UV and blue light simultaneously, ϕ_a quickly reaches a steady state. Therefore, r_{low} is thought to be the activation rate of OPN5 by short-wavelength light emitted by UCNPs, r_{high} is the activation rate of OPN5 by UV light, and r_{mid} is the activation rate of OPN5 by NIR light (the mechanism is currently unknown).

Based on this result, we will consider case 4 and the remaining half of the cells in case 3, which belong to the r_{mid} group. In case 3, there are almost equal numbers of cells in which OPN5 is activated mainly by the emission of UCNPs and cells in which OPN5 is directly activated by NIR light. In case 4, although there are many UCNPs in the dish, they are not bound to cells, so the emission of UCNPs is not strong enough to activate OPN5, and it is thought that most activation was by NIR light. From these results, it was found that it is possible to activate the bistable opsin OPN5 using UCNPs that emit light at both the activation and deactivation wavelengths simultaneously, but that the activation efficiency is better when the UCNPs are bound to cells in the vicinity of OPN5.

Source of biological samples

HEK293T cell line was purchased from RIKEN BioResource Research Center. We constructed the plasmid encoding human OPN5 with an extracellular FLAG tag ourselves. ANTI-FLAG BioM2–biotin antibody (#F9291) and monoclonal ANTI-FLAG M2 antibody (#F1804) were purchased from Sigma-Aldrich. Goat anti-mouse IgG (H + L) cross-adsorbed secondary antibody with Alexa Fluor 594 (#A-11005) was obtained from Invitrogen.

Conclusions

In this study, the activation of OPN5 – a model bistable opsin activated by UV light and deactivated by blue light – through emission from UCNPs excited by NIR light was demonstrated. Specifically, we conjugated $NaYF_4$:Yb,Tm@$NaLuF_4$ core–shell UCNPs to OPN5-expressing HEK293T cells, irradiated them with NIR light, and observed the cellular Ca^{2+} response. The results showed that, even though the emission of UCNPs includes not only UV light but also blue light of equal or greater intensity, it can still activate OPN5. This study provides the first experimental evidence of non-invasive and spatially precise light control of GPCR-type bistable opsins using UCNPs, opening new avenues for light manipulation of deep tissues and functional studies of bistable opsins in complex biological systems.

Author contributions

The work was initiated by S. M.; F. K. and S. M. devised the method; F. K. constructed the experimental setup and performed all the experiments under the supervision of M. T., Y. H., K. M., D. K. and S. M.; K. H. conducted STEM observation of UCNPs; Y. H. assisted in the plasmid design and construction; K. M. supported cell experiments; D. K. provided technical advice for the Ca^{2+} imaging experiment; F. K. and S. M. drafted the manuscript. All authors reviewed the manuscript and have given approval to the final version of the manuscript.

Conflicts of interest

There are no conflicts to declare.

Data availability

The data supporting this article have been included as part of the supplementary information (SI). Supplementary information is available. See DOI: https://doi.org/10.1039/d5na01109d.

Acknowledgements

This work was supported by JST SPRING, Japan Grant Number JPMJSP2102 and the Sasakawa Scientific Research Grant from The Japan Science Society. This work was partially supported by Harmonic Ito Foundation. F. K. would like to thank Dr Matomo Sakari for his useful advice on cell experiments, including transfection. We would like to express our gratitude to Ms Chiharu Tatsumi from JAIST for her help with the plasmid construction and preparation and to Prof. Kenzo Fujimoto from JAIST for lending us the UV LED. We would like to thank Simon Moore for his assistance in proofreading the manuscript.

References

1 E. S. Boyden, F. Zhang, E. Bamberg, G. Nagel and K. Deisseroth, *Nat. Neurosci.*, 2005, **8**, 1263–1268.
2 J. A. Cardin, M. Carlén, K. Meletis, U. Knoblich, F. Zhang, K. Deisseroth, L.-H. Tsai and C. I. Moore, *Nat. Protoc.*, 2010, **5**, 247–254.
3 S. R. Pulver, N. J. Hornstein, B. L. Land and B. R. Johnson, *Adv. Physiol. Educ.*, 2011, **35**, 82–91.
4 A. Dawydow, R. Gueta, D. Ljaschenko, S. Ullrich, M. Hermann, N. Ehmann, S. Gao, A. Fiala, T. Langenhan, G. Nagel and R. J. Kittel, *Proc. Natl. Acad. Sci. U. S. A.*, 2014, **111**, 13972–13977.
5 X. Han and E. S. Boyden, *PLoS One*, 2007, **2**, e299.
6 A. B. Arrenberg, F. Del Bene and H. Baier, *Proc. Natl. Acad. Sci. U. S. A.*, 2009, **106**, 17968–17973.

7 E. Ritter, K. Stehfest, A. Berndt, P. Hegemann and F. J. Bartl, *J. Biol. Chem.*, 2008, **283**, 35033–35041.
8 C. Bamann, T. Kirsch, G. Nagel and E. Bamberg, *J. Mol. Biol.*, 2008, **375**, 686–694.
9 J. Hu, Y. Shi, J. Zhang, X. Huang, Q. Wang, H. Zhao, J. Shen, Z. Chen, W. Song, P. Zheng, S. Zhan, Y. Sun, P. Cai, K. An, C. Ouyang, B. Zhao, Q. Zhou, L. Xu, W. Xiong, Z. Zhang, J. Meng, J. Chen, Y. Ma, H. Zhao, M. Zhang, K. Qu, J. Hu, M. Luo, F. Xu, X. Chen, Y. Xiong, J. Bao and T. Xue, *Cell*, 2022, **185**, 3124–3137.
10 O. N. Ekechukwu and M. Christian, *Rev. Endocr. Metab. Disord.*, 2022, **23**, 111–120.
11 L. L. Ospri, G. Prusky and S. Hattar, *Annu. Rev. Neurosci.*, 2017, **40**, 539–556.
12 D. Basili, G. Gioacchini, V. Todisco, M. Candelma, L. Marisaldi, L. Pappalardo and O. Carnevali, *Gen. Comp. Endocrinol.*, 2021, **303**, 113707.
13 M. Koyanagi and A. Terakita, *Biochim. Biophys. Acta*, 2014, **1837**, 710–716.
14 M. Zhang, T. Chen, X. Lu, X. Lan, Z. Chen and S. Lu, *Signal Transduct. Targeted Ther.*, 2024, **9**, 88.
15 A. Terakita, *Genome Biol.*, 2005, **6**, 213.
16 K.-W. Yau and R. C. Hardie, *Cell*, 2009, **139**, 246–264.
17 B. Rayer, M. Naynert and H. Stieve, *J. Photochem. Photobiol., B*, 1990, **7**, 107–148.
18 *Encyclopedia Britannica*, https://www.britannica.com/science/rhodopsin, accessed April 2025.
19 H. Tsukamoto and A. Terakita, *Photochem. Photobiol. Sci.*, 2010, **9**, 1435–1443.
20 S. M. Spangler and M. R. Bruchas, *Curr. Opin. Pharmacol.*, 2017, **32**, 56–70.
21 N. Abreu and J. Levitz, *Methods Mol. Biol.*, 2020, **2173**, 21–51.
22 J. Wietek, A. Nozownik, M. Pulin, I. Saraf-Sinik, N. Matosevich, R. Gowrishankar, A. Gat, D. Malan, B. J. Brown, J. Dine, B. N. Imambocus, R. Levy, K. Sauter, A. Litvin, N. Regev, S. Subramaniam, K. Abrera, D. Summarli, E. M. Goren, G. Mizrachi, E. Bitton, A. Benjamin, B. A. Copits, P. Sasse, B. R. Rost, D. Schmitz, M. R. Bruchas, P. Soba, M. Oren-Suissa, Y. Nir, J. S. Wiegert and O. Yizhar, *Nat. Methods*, 2024, **21**, 1275–1287.
23 Z. Melyan, E. E. Tarttelin, J. Bellingham, R. J. Lucas and M. W. Hankins, *Nature*, 2005, **433**, 741–745.
24 K. Spoida, D. Eickelbeck, R. Karapinar, T. Eckhardt, M. D. Mark, D. Jancke, B. V. Ehinger, P. König, D. Dalkara, S. Herlitze and O. A. Masseck, *Curr. Biol.*, 2016, **26**, 1206–1212.
25 M. Koyanagi, E. Kawano, Y. Kinugawa, T. Oishi, Y. Shichida, S. Tamotsu and A. Terakita, *Proc. Natl. Acad. Sci. U. S. A.*, 2004, **101**, 6687–6691.
26 T. Yamashita, H. Ohuchi, S. Tomonari, K. Ikeda, K. Sakai and Y. Shichida, *Proc. Natl. Acad. Sci. U. S. A.*, 2010, **107**, 22084–22089.
27 D. Kojima, S. Mori, M. Torii, A. Wada, R. Morishita and Y. Fukada, *PLoS One*, 2011, **6**, e26388.
28 E. E. Tarttelin, J. Bellingham, M. W. Hankins, R. G. Foster and R. J. Lucas, *FEBS Lett.*, 2003, **554**, 410–416.
29 X. Jiang, M. T. Pardue, K. Mori, S.-I. Ikeda, H. Torii, S. D'Souza, R. A. Lang, T. Kurihara and K. Tsubota, *Proc. Natl. Acad. Sci. U. S. A.*, 2021, **118**, e2018840118.
30 K. X. Zhang, S. D'Souza, B. A. Upton, S. Kernodle, S. Vemaraju, G. Nayak, K. D. Gaitonde, A. L. Holt, C. D. Linne, A. N. Smith, N. T. Petts, M. Batie, R. Mukherjee, D. Tiwari, E. D. Buhr, R. N. Van Gelder, C. Gross, A. Sweeney, J. Sanchez-Gurmaches, R. J. Seeley and R. A. Lang, *Nature*, 2020, **585**, 420–425.
31 A. Fukuda, K. Sato, C. Fujimori, T. Yamashita, A. Takeuchi, H. Ohuchi, C. Umatani and S. Kanda, *Science*, 2025, **387**, 43–48.
32 C. Ash, M. Dubec, K. Donne and T. Bashford, *Laser Med. Sci.*, 2017, **32**, 1909–1918.
33 G. Chen, Y. Cao, Y. Tang, X. Yang, Y. Liu, D. Huang, Y. Zhang, C. Li and Q. Wang, *Adv. Sci.*, 2020, **7**, 1903783.
34 S. Pearson, J. Feng and A. del Campo, *Adv. Funct. Mater.*, 2021, **31**, 2105989.
35 R. Weissleder, *Nat. Biotechnol.*, 2001, **19**, 316–317.
36 S. Shah, J.-J. Liu, N. Pasquale, J. Lai, H. McGowan, Z. P. Pang and K.-B. Lee, *Nanoscale*, 2015, **7**, 16571–16577.
37 X. Ai, L. Lyu, Y. Zhang, Y. Tang, J. Mu, F. Liu, Y. Zhou, Z. Zuo, G. Liu and B. Xing, *Angew. Chem., Int. Ed.*, 2017, **56**, 3031–3035.
38 S. Chen, A. Z. Weitemier, X. Zeng, L. He, X. Wang, Y. Tao, A. J. Y. Huang, Y. Hashimotodani, M. Kano, H. Iwasaki, L. K. Parajuli, S. Okabe, D. B. L. Teh, A. H. All, I. Tsutsui-Kimura, K. F. Tanaka, X. Liu and T. J. McHugh, *Science*, 2018, **359**, 679–684.
39 J. Yan, Y. Wan, Z. Ji, C. Li, C. Tao, Y. Tang, Y. Zhang, Y. Liu and J. Liu, *Adv. Funct. Mater.*, 2023, **33**, 2303992.
40 D. Maemura, T. S. Le, M. Takahashi, K. Matsumura and S. Maenosono, *ACS Appl. Mater. Interfaces*, 2023, **15**, 42196–42208.
41 X. Ai, C. J. H. Ho, J. Aw, A. B. E. Attia, J. Mu, Y. Wang, X. Wang, Y. Wang, X. Liu, H. Chen, M. Gao, X. Chen, E. K. L. Yeow, G. Liu, M. Olivo and B. Xing, *Nat. Commun.*, 2016, **7**, 10432.
42 A. Qu, X. Wu, S. Li, M. Sun, L. Xu, H. Kuang and C. Xu, *Adv. Mater.*, 2020, **32**, e2000184.
43 C. Chen, F. Wang, S. Wen, Q. P. Su, M. C. L. Wu, Y. Liu, B. Wang, D. Li, X. Shan, M. Kianinia, I. Aharonovich, M. Toth, S. P. Jackson, P. Xi and D. Jin, *Nat. Commun.*, 2018, **9**, 3290.
44 X. Zeng, S. Chen, A. Weitemier, S. Han, A. Blasiak, A. Prasad, K. Zheng, Z. Yi, B. Luo, I.-H. Yang, N. Thakor, C. Chai, K.-L. Lim, T. J. McHugh, A. H. All and X. Liu, *Angew. Chem., Int. Ed.*, 2019, **58**, 9262–9268.
45 J. Peng, W. Xu, C. L. Teoh, S. Han, B. Kim, A. Samanta, J. C. Er, L. Wang, L. Yuan, X. Liu and Y.-T. Chang, *J. Am. Chem. Soc.*, 2015, **137**, 2336–2342.
46 X. Ai, Z. Wang, H. Cheong, Y. Wang, R. Zhang, J. Lin, Y. Zheng, M. Gao and B. Xing, *Nat. Commun.*, 2019, **10**, 1087.
47 F. Wang, R. Deng, J. Wang, Q. Wang, Y. Han, H. Zhu, X. Chen and X. Liu, *Nat. Mater.*, 2011, **10**, 968–973.
48 W. Yang, X. Li, D. Chi, H. Zhang and X. Liu, *Nanotechnology*, 2014, **25**, 482001.

49 S. Wu, X.-J. Kong, Y. Cen, J. Yuan, R.-Q. Yu and X. Chu, *Nanoscale*, 2016, **8**, 8939–8946.
50 X. Lin, X. Chen, W. Zhang, T. Sun, P. Fang, Q. Liao, X. Chen, J. He, M. Liu, F. Wang and P. Shi, *Nano Lett.*, 2018, **18**, 948–956.
51 L. M. Wiesholler, C. Genslein, A. Schroter and T. Hirsch, *Anal. Chem.*, 2018, **90**, 14247–14254.
52 S. Wen, J. Zhou, K. Zheng, A. Bednarkiewicz, X. Liu and D. Jin, *Nat. Commun.*, 2018, **9**, 2415.
53 A. Karami, T. J. de Prinse, N. A. Spooner, S. P. Kidd, C. J. Sumby and J. Bi, *ACS Appl. Nano Mater.*, 2023, **6**, 7031–7043.
54 N. T. Nguyen, J. Kim, X. T. Le, W. T. Lee, E. S. Lee, K. T. Oh, H.-G. Choi and Y. S. Youn, *ACS Nano*, 2023, **17**, 382–401.
55 R. Arppe, I. Hyppänen, N. Perälä, R. Peltomaa, M. Kaiser, C. Würth, S. Christ, U. Resch-Genger, M. Schäferling and T. Soukka, *Nanoscale*, 2015, **7**, 11746–11757.
56 A. Vernay and P. Cosson, *BMC Res. Notes*, 2013, **6**, 317.
57 T. Sugiyama, H. Suzuki and T. Takahashi, *Sci. Rep.*, 2014, **4**, 5352.
58 W. L. Shen, Y. Kwon, A. A. Adegbola, J. Luo, A. Chess and C. Montell, *Science*, 2011, **331**, 1333–1336.
59 G. Palczewska, F. Vinberg, P. Stremplewski, M. P. Bircher, D. Salom, K. Komar, J. Zhang, M. Cascella, M. Wojtkowski, V. J. Kefalov and K. Palczewski, *Proc. Natl. Acad. Sci. U. S. A.*, 2014, **111**, E5445–E5454.
60 K. Sato, T. Yamashita and H. Ohuchi, *J. Biol. Chem.*, 2023, **299**, 105020.
61 E. J. Dickson, B. H. Falkenburger and B. Hille, *J. Gen. Physiol.*, 2013, **141**, 521–535.